1 2 3 4 5 6 7 8	Word counts Introduction: 1283 Materials and Methods: 1868 Results: 1034 Discussion: 2574 Total: 6759 Number of figures: 6
10	Number of tables: 1
11 12	Number of SI: 4
13	
14	Insights into source/sink controls on wood
15	formation and photosynthesis from a stem
16	chilling experiment in mature red maple
17 18 19 20 21 22 23 24	Tim Rademacher*,1,2,3, Patrick Fonti ⁴ , James M. LeMoine ² , Marina V. Fonti ^{4,5} , Francis Bowles ⁶ , Yizhao Chen ⁷ , Annemarie H. Eckes-Shephard ^{7,8} , Andrew D., Friend ⁷ , and Andrew D. Richardson ² *Corresponding author: tim.rademacher@uqo.ca ¹ Harvard Forest, Harvard University, Petersham, Massachusetts, USA. ² School of Informatics, Computing and Cyber Systems and Center for Ecosystem Science and Society, Northern Arizona
21 22 23 24 25 26 27 28 29 30 31	University, Flagstaff, Arizona, USA. 3 Institut des Sciences de la Forêt Tempérée, Université du Québec en Outaouais, Ripon, Québec, Canada. 4 Swiss Federal Research Institute for Forest, Snow and Landscape Research WSL, Birmensdorf, Switzerland. 5 Institute of Ecology and Geography, Siberian Federal University, Krasnoyarsk, Russian Federation 6 Research Designs, Lyme, New Hampshire, USA. 7 Department of Geography, University of Cambridge, Cambridge, Cambridgeshire, UK. 8 Department of Physical Geography and Ecosystem Science, Lund University, Lund, Sweden.
32	Summary
33	Whether sources or sinks control wood growth remains debated with a paucity of
34	evidence from mature trees in natural settings.
35	Here, we altered carbon supply rate in stems of mature red maples (Acer rubrum)
36	within the growing season by restricting phloem transport using stem chilling; thereby
37	increasing carbon supply above and decreased carbon supply below the restrictions,
38	respectively.
39	Chilling successfully altered nonstructural carbon concentrations (NSC) in the

phloem without detectable repercussions on bulk NSC in stems and roots. Ring width

responded strongly to local variations in carbon supply with up to seven-fold differences

40

along the stem of chilled trees; however, concurrent changes in the structural carbon were inconclusive at high carbon supply due to large local variability of wood growth. Above chilling-induced bottlenecks, we also observed higher leaf NSC concentrations, reduced photosynthetic capacity, and an advancement of leaf coloration and fall.

Our results indicate that the cambial sink (particularly cell division) is affected by carbon supply, but within-tree feedbacks can downregulate source activity, when carbon supply to the cambium exceeds demand. Because such feedbacks have so far only been hypothesized in mature trees, these findings constitute an important advance in understanding source-sink dynamics and suggest that mature red maples operate close to both source- and sink-limitation.

Keywords: Anatomy, Growth, Nonstructural carbon, Phloem, Source, Sink, Wood, Xylogenesis.

Introduction

Wood—the secondary xylem and defining feature of trees—is a remarkable material. It shapes ecosystems, by enabling trees to grow tall and compete for light (Niklas, 1992); it has altered the developmental trajectory of the biosphere and earth system by serving as a slow-turnover pool of organic matter, thus sequestering atmospheric CO₂ (Pugh *et al.*, 2020); and, it has influenced the evolution of human societies and civilization by providing fuel, fiber, and building materials that are strong and light (Brostow *et al.*, 2010). However, wood is in some ways a conundrum: while dendrochronologists, schoolchildren, and foresters all know that trees grow more in some years and less in others (Fritts, 2012), our mechanistic understanding of the underlying processes controlling interannual variation in wood growth is surprisingly poor, especially with regard to mature trees growing in natural settings (Rathgeber *et al.*, 2016; Friend *et al.*, 2019).

There are two ways in which environmental factors might influence wood growth (xylogenesis) and these are reflected in the two dominant paradigms: either wood growth is controlled by carbon supply—from current photosynthesis, which may be supplemented from reserves— i.e. "source-limited," or wood growth is controlled by the activity of the lateral meristem, through the direct impact of limiting (environmental or internal) factors on the processes of xylogenesis, i.e. "sink-limited" (Körner, 2003). The source-limited hypothesis is the basis of most vegetation models (Fatichi *et al.*, 2014; Körner, 2015; Friend *et al.*, 2019), but there is more and more evidence for direct environmental limitations on the cambium (Körner, 2006; Parent *et al.*, 2010; Peters *et al.*, 2020). A consequence of the sink-limited hypothesis is the existence of feedback mechanisms from sinks to sources that will cause source activity

(photosynthesis) to be down-regulated when sink activity (xylogenesis) is inadequate to meet supply (Walker *et al.*, 2021).

While distinguishing between source- and sink-limitation might seem straightforward, in practice it is not (Gessler & Grossiord, 2019). This is because at either extreme, xylogenesis must be either source- or sink-limited. Clearly carbon supply must be a top-down constraint on growth, as wood growth can never exceed carbon supply. However, at the same time there must be an upper limit on growth (G_{max} ; Fig. 1A), controlled by the maximum sink activity and independent of carbon supply. What is needed are experimental designs that offers the opportunity to identify whether under ambient environmental conditions source- or sink-limitation is dominant in various species and ecosystems? Conceptually, a tree could operate under either limitation and possibly switch between them over time (Fig. 1A). In this framework, a transition from supply-limited growth to sink-limited growth occurs at a supply level of C* (Fig. 1A). With our present knowledge of carbon dynamics and xylogenesis, however, it is not known whether trees are more generally operating below C* (where growth is supply-limited, e.g. C_1), above C* (where growth is sink-limited, e.g. C_2), or in fact close to C* possibly switching between supply- and sink-limitation over time.

Previous studies have provided mixed results in support of these competing views. Girdling experiments, which show reductions in growth below the girdle (reduced supply) and increases in growth above the girdle (enhanced supply), suggest that wood growth is supply-limited (Wilson, 1968; Maier *et al.*, 2010). But, at the whole-tree level, CO₂ enrichment, which would be expected to enhance carbon supply to the entire tree because of stimulated photosynthesis, has not generally been shown to result in increased wood growth in mature trees (Körner *et al.*, 2005; Jiang *et al.*, 2020; Lauriks *et al.*, 2021), supporting the sink-limitation hypothesis (and pointing to within-tree feedbacks down-regulating photosynthetic activity). Other experimental studies have equally shown that wood growth is reduced following exposure to low atmospheric CO₂ (Huang *et al.*, 2021), experimentally induced defoliation (Deslauriers *et al.*, 2015; Wiley *et al.*, 2017), as well as natural defoliation resulting from pest outbreaks (Castagneri *et al.*, 2020). However, these growth responses could simply result from severe supply-limitation (e.g. C₁): they tell us nothing about whether sink-limitation occurs more generally.

Here, we used an experimental manipulation—applying the "phloem chilling" method of Johnsen et al. (2007) and de Schepper et al. (2011)—to regulate the carbon flow to different points along the stem of mature red maples (*Acer rubrum*). As phloem flow is modulated by temperature (Jensen et al., 2016), phloem transport can be temporarily and reversibly blocked by chilling the phloem close to 0°C (Gould et al., 2004; Peuke et al., 2006; Thorpe et al., 2010). An advantage of this approach is that unlike traditional girdling approaches, phloem chilling does not cause wounding and is reversible (Rademacher et al., 2019). We installed chilling collars at 1.0 and 2.0 m to create a gradient of carbon supply along the stem

and isolate one stem section (between 1 and 2 m) from both recent assimilates from the canopy and root reserves (Fig. 1B). Our focus here is on this alteration of carbon supply below, between, and above the transport restrictions, rather than on the growth response under each collar (e.g., 1 and 2 m), where nearfreezing temperatures constitute an acute limitation (Fig. 1D). We used microcores to observe the seasonal progression of xylogenesis, and we also characterised stem respiration and concentrations of stored nonstructural carbon (NSC) to quantify local carbon dynamics. Leaf-level measurements of photosynthesis, and visual observations of leaf phenology (i.e., bud burst, leaf elongation, leaf colouration, and leaf fall) were used to assess the impact of any within-tree feedback mechanisms. Ultimately, whether a tree is source- or sink-limited may vary over time, especially when differences in source and sink phenologies may cause temporary carbon surpluses or deficits in shoulder seasons. Here, we focused on the early growing season (29th May to 10th July 2019), when trees appear to be particularly sensitive to phloem transport manipulations (Maier et al., 2010; De Schepper et al., 2011). Based on the concepts presented above (Fig. 1A), we hypothesized that if wood growth is supply-limited (C₁), then in our experimental treatments we should see reductions of growth at 1.5 m (the isolated stem section) and possibly at 0.5 m (depending on root reserve depletion) but enhancements of growth at 2.5 m (Conclusion: Reject sink-limited hypothesis, under current environmental conditions). If on the other hand wood growth is sink-limited (C₂), then our experimental treatments should neither lead to reduced growth at 1.5 m and 0.5 m (as long as root reserves are not depleted) nor enhanced growth at 2.5 m (Conclusion: Reject supply-limited hypothesis, under current environmental conditions). A third possibility is that under current environmental conditions, trees are operating in the vicinity of C*. In this case, we might see reduced growth at 1.5 m in response to reduced carbon supply, but no response at 2.5 m in response to enhanced carbon supply (Conclusion: joint limitation of growth by supply-limitation and sink-limitation). Finally, feedbacks could downregulate source activity (evidenced through potential changes in photosynthetic activity and/or leaf phenology) as a result of the build-up of phloem carbon above the top chilling collar (Conclusion: Within-tree feedbacks can modulate photosynthesis to control supply in response to demand). We expect that all treatment effects will gradually accumulate during the chilling treatment, but will taper off after the chilling is ended (i.e., after the peak growing season to avoid the complete halt of wood growth; Fig. 1C). Understanding the role of source-sink dynamics of large trees in natural settings under ambient environmental conditions is important because of their importance as a sink in the global carbon cycle (Pugh et al., 2019) and the fact that source-sink interactions in large trees are different from small trees (Hartmann et al., 2018). Our experiment provides a rare look into the source-sink interactions of mature trees in a natural temperate forest.

108

109

110

111

112

113

114

115

116

117

118119

120

121

122

123

124

125

126

127

128

129

130

131

132

133

134

135

136

137

138

139

140

Materials and Methods

Study site and species

Red maple (*Acer rubrum*) is widespread throughout eastern North America, and of great cultural and commercial importance. At Harvard Forest in central Massachusetts, USA, red maple is together with red oak the most dominant species in a mixed forest. We studied a cohort of eight mature trees growing in close proximity (within 20 m of each other) in the Prospect Hill Tract (42°30.8' N, 72°13.1' W, 350m above sea level) on sandy acidic loam. These 75±1.7 (μ±σ) year-old trees regenerated naturally after a stand-replacing hurricane in 1938. They have experienced an average temperature of 8.0±0.7°C and annual precipitation of 1096±228 mm over the past 57 years (Boose & Gould, 2019) reaching an average diameter of breast height of 24.2±1.2 cm and a mean height of 22.6±1.0 m. The experiment was performed in 2019, a relatively wet year with 270 mm above the average of the instrumental record and directly followed the wettest year on record with 1840 mm. Annual mean temperature in 2019 was close to the long-term average with 7.9°C. Overall, neither the preceding year, nor the year of the experiment, showed strong climatic constraints.

157 Chilling setup

We separated the cluster of eight trees into four pairs, with each two trees of similar size and canopy status (SI 1). We flipped a coin to randomise which tree of each pair was subjected to phloem chilling at 1.0 and 2.0m (Fig. 1B). To monitor phloem temperatures, negative temperature coefficient thermistors (2.5 mm diameter, SC30F103V, Amphenol Thermometrics Inc., St. Marys, Pennsylvania, USA) were placed into the phloem, one each at 1.0 and 2.0 m using surgical needles in early May 2019. Around the same time, we also installed heat-pulse sap flow sensors (East 30, Pullman, Washington, USA) at 1.5 m, which measure sap flow at three depths (i.e., 5.0, 17.5, and 30.0 mm). In mid-May, we wrapped 3/8" type L copper tubing 30 times around stems to produce 30-cm-wide chilling collars (centered on the chilling height), which were linked to a coolant supply line using one ALPHA2 circulator (Grundfos, Bjerringbro, Denmark) for each tree (i.e., supplying two chilling collars). To chill the trees, coolant - a mix of water and polypropylene glycol - was constantly circulated through the main supply line and the chilling collars from a reservoir that was cooled to maintain a temperature of roughly 0°C with a six-ton chiller using a 1.5 horse power circulation pump (Chillking, Bastrop, Texas, USA). During the chilling period, 20 thermistors (T 109, Campbell Scientific, Logan, Utah, USA), which were calibrated in an ice-bath prior

to deployment, were used to monitor air temperature, temperatures of the supply lines, and at the chilling collars. Piping and chilling collars were insulated (e.g., bubble wrap, glass wool, piping insulation) and covered in radiative barriers. The chilling was switched on at midday on 29 May 2019 and switched off at midday on 10 Jul 2019, reducing phloem temperatures to an average of $2.8\pm2.6^{\circ}$ C at 1.0 m and 1.4 ± 1.8 at 2.0 m in chilled trees over this 42-day period. Phloem temperatures in chilled trees at 1.0 and 2.0 m were 15.4 and 16.8° C lower than the control group during this chilling period, but only 2.3° C lower at 1.5 m, suggesting that the chilling effects were mainly local but there was some diffusion (i.e., mostly up stem with xylem sap flow during the day). At 1.5 m phloem temperature of control trees closely followed air temperature ($R^2 = 0.98$). During the chilling, phloem temperatures at 1.0 and 2.0 m were maintained in the range of 0 to 5° C for 84 and 97% of the time.

Physiological monitoring

172

173

174

175

176

177

178

179

180

181

182

183

184

185

186

187

188

189

190

191

192

193

194

195

196

197

198

199

200

201

202

203

204

We monitored wood formation and resulting anatomy, NSC concentrations in leaves, stems and roots, stem CO₂ efflux, sap flow, leaf phenology, as well as leaf and branch water potential throughout the 2019 growing season (Fig. 1B). Wood formation was assessed from thin-section (7 µm-thick cross-sectional cuts), which were obtained from microcores at 0.5, 1.5, 2.5, and 4.0 m throughout the 2019 growing season (see Fig. 2A for sampling dates) and one follow-up sample on 4 Aug 2020. Microcores were stored in a solution of 75% ethanol and 25% glacial acetic acid for 24 hours after collection. Then, they were transferred to 95% ethanol until they were embedded in paraffin (Tissue Processor 102, Leica Biosystems, Germany), stained with astra-blue and safranin, and cut with a rotary microtome (RM2245, Leica Biosystems, Wetzlar, Germany). Images of the thin-sections were scanned at a resolution of circa 1.5 pixels per µm (Axioscan Z1, Zeiss, Jena, Germany) and ring widths were measured using the Wood Image Analysis and Database (Rademacher et al., 2021c; Seyednasrollah et al., 2021). To compare differences in growth between sampling locations, we fitted monotonic general additive models to each growth series using the scam v1.2-9 package (Pya, 2020). For each growth series, we identified the start of wood formation as the date halfway between the sampling dates of the last microcore without and the first microcore with signs of cell enlargement. To estimate the cell-wall area in one end-of-season image, we converted a region of interest for the 2018 and 2019 ring to greyscale and used a threshold to differentiate between lumen areas and cell-wall areas. Regions of interest were maximised for each ring, while excluding rips and tears in the sample. We reported results for a brightness threshold of 0.8, but varying thresholds between 0.7 to 0.9 did not change the reported patterns. Cell-wall area estimates were converted to mass using a cell-wall density of 1.459 g cm⁻³ for red maple (Kellogg & Wangaard, 1969). Vessels were identified in each region of interest after denoising the image using the determinant of Hessian operator (Lindeberg, 2015) as implemented in the *imhessian* function of the *imager* package

205 (Barthelme, 2020). We added a minimum size threshold of 500 µm² to differentiate between large fiber 206 lumina and small vessel lumina. An illustration of the methods can be found in the supplements (SI 4). 207 208 For NSC analysis, we collected tissue samples from roots, stems at 0.5, 1.5, and 2.5 m and sun-exposed 209 leaves throughout the growing season, froze them on dry ice, transferred them to a freezer (-60°C) as soon 210 as possible, before they were eventually freeze-dried (FreeZone 2.5, Labconco, Kansas City, USA with a 211 Hybrid Vacuum Pump, Vaccubrand, Wertheim, Germany), ground (mesh 20, Thomas Scientific Wiley 212 Mill, Swedesboro, New Jersey, USA), and homogenised (SPEX SamplePrep 1600, MiniG, Metuchen, 213 New Jersey, USA). Root and stem samples were collected using an increment corer (5.15 mm, Hagöf, 214 Långele, Sweden), while several sun-exposed leaves were cut with pruning shears from a bucket lift. For 215 roots, we sampled one large coarse root per tree repeatedly at least 1m below the root collar and 15 cm 216 from any previous sampling location. All the xylem tissue was homogenised for each root sample. For 217 stem samples, we separated phloem (i.e., whole phloem area), the outer bark, and the first centimetre of 218 the xylem and homogenised them separately. We used an established protocol for colorimetric analysis of 219 soluble sugar and starch concentrations using phenol-sulphuric acid after ethanol extraction (Landhäusser 220 et al., 2018). Absorbances were read twice for each sample at 490 nm for sugar and 525 nm for starch 221 using a spectrophotometer (GENESYS 10S UV-Vis, Thermo Fisher Scientific, Waltham, Massachusetts, 222 USA). To calibrate absorbance measurements with 1:1:1 glucose:fructose:galactose curves (Sigma 223 Chemicals, St. Louis, Missouri, USA) we used the R package NSCprocessR 224 (https://github.com/TTRademacher/NSCprocessR). For overall quality control, we used laboratory 225 control standards of red oak stem wood (Harvard Forest, Petersham, Massachusetts, USA) and potato 226 starch (Sigma Chemicals, St. Louis, Missouri, USA). Batches of 40 samples always included at least 227 seven blanks and nine laboratory control standards. The control standards had coefficients of variation of 228 0.08 and 0.12 for red oak soluble sugar and starch concentrations and 0.07 for potato starch. 229 230 To quantify the relationship between chilling and basic tree metabolism, we also measured stem CO₂ 231 efflux. Every week throughout the growing season, we measured CO₂ efflux at 0.5, 1.5, and 2.5 m on all 232 trees starting at 13:00 GMT-4 and normally took less than an hour. We measured chambers in the same 233 order to facilitate comparison over longer time scales by minimising difference in diurnal fluctuations. 234 CO₂ concentrations were measured with a closed-chamber attached to a Infra-red gas analyser (Li-820, 235 LI-COR, Lincoln, Nebraska, USA) at 1Hz once the chamber internal CO₂ concentration had stabilised at 236 ambient levels (Carbone et al., 2019) and converted to fluxes with uncertainties using the 237 RespChamberPro package (Perez-Priego et al., 2015). 238

We monitored the leaf phenology of all eight red maples, plus six additional red maples in the stand in 2018 and 2019 according to the protocol by O'Keefe (2019). Using binoculars, we visually observed the crown of each tree to determine the dates of bud burst, leaf elongation, leaf colouration, and leaf fall. During the period with green leaves, we also measured pre-dawn leaf and branch water potential approximately every second week to estimate potential effects of the chilling on tree water status (in addition to the sap flow sensors; SI 3).

During the last ten days of the chilling, we conducted a campaign to compare photosynthesis and chlorophyll fluorescence in chilled and control trees (purple highlight in Fig. 1C & D). Instantaneous photosynthetic rates (n = 46), light response curves, and A/Ci curves were measured in shade or sun leaves of each pair of trees (i.e., one control and one chilled tree) simultaneously using two LICOR-6400 (Lincoln, Nebraska, USA) from a bucket lift. We estimated photosynthetic parameters (maximal rate of photosynthetic electron transport or J_{max} and maximal rate of RuBisCO carboxylation activity or V_{cmax}), by fitting A/Ci curves to the data using the *plantecophys* package (Duursma, 2015). Directly after each photosynthesis measurement, we also removed the leaf and measured chlorophyll fluorescence (OS-30P, Opti-Sciences, Hudson, New Hampshire, USA). Then, we wrapped each leaf in aluminium foil and kept it in a cooler with ice to dark-adapt. In the evening of each day, we re-measured chlorophyll fluorescence in dark-adapted leaves, to estimate stress to the photosynthetic apparatus (Maxwell & Johnson, 2000).

Statistical analysis

All statistical analyses were performed in R v3.6.3 (R Core Team, 2019). The data and code to reproduce all results are publicly available on the Harvard Forest Data Archive (Rademacher *et al.*, 2021b). We used mixed effects models that were fitted using the *lme4* package (Bates *et al.*, 2015) with tree identifiers as a random variable, and a fixed treatment effect. For data with various data points along the stem, we include a sampling height and treatment interaction as a proxy carbon supply gradient. When measurement series over time were compared, we also include datetime as a categorical fixed effect and its interaction with the treatment or the treatment and sampling height interactive effect in the case of stem data. We refrain from reporting significance based on arbitrary p-values in line with the philosophy of the *lme4* package, as the degrees of freedom of mixed effects models are non-trivial and can only be estimated (Bates *et al.*, 2015). Instead, we report estimated mean effects and their standard errors ($\hat{\mu}\pm\hat{\sigma}_{\hat{\mu}}$) as well as relative differences between these (in %) unless specified otherwise and leave it to the reader to decide on their significance.

272 Results

303

273 Changes to carbon supply and NSC concentrations 274 We altered phloem transport by chilling stem sections as shown by changes in local phloem sugar 275 concentrations. Phloem sugar concentrations were similar between treatment groups before chilling, but 276 increased above the chilling collars (Fig. 3A). Phloem sugar concentration increased during the chilling 277 by 13% (0.35±0.35% dry weight), 18% (0.50±0.35% dry weight), and 34% (0.92±0.36% dry weight) at 278 0.5, 1.5, and 2.5 m, respectively. In contrast, phloem starch concentrations increased above the chilling 279 collars by an average 37% during the chilling treatment (0.25±0.20% dry weight) and decreased by 64% 280 below the two chilling collars (0.43±0.18% dry weight). It is likely that some starch was remobilised to 281 supplement phloem sugar depleted as a result of the flow restrictions. While NSC concentrations in the 282 phloem, particularly soluble sugar, showed treatment effects (Fig. 3A), bulk NSC concentrations in stems 283 and roots across the first centimetre of xylem tissue varied comparatively little between the control and 284 chilled trees before, during and after the chilling (Fig. 4). 285 286 Changes to wood growth 287 The chilling-induced restriction of phloem transport affected radial wood growth along the stem, with 288 wider rings forming in regions of increased carbon supply and narrower rings forming in regions of 289 reduced carbon supply (Fig. 2A & B). Over the five preceding years and the following year, both control 290 and chilled trees showed little pre-existing variation in growth with sampling height (standard deviation 291 of 0.1 mm and 0.2 mm for control and chilled groups). Control trees continued to grow without 292 systematic variation with sampling height at an average ring width of 1.9±0.6 mm in 2019 (Fig. 2B). 293 Chilled trees grew 84% less below the two phloem restrictions (0.3±0.1 mm), 26% less below one phloem 294 restriction (1.4±0.3 mm), and 16 to 21% more above the restrictions (2.2±1.0 mm at 2.5 and 2.3±0.9 mm 295 at 4 m). Despite the more than 7-fold difference in ring width between 4.0 m and 0.5 m in chilled trees 296 (difference in mean estimated effect from mixed effects model), intra-annual growth dynamics (i.e., 297 general shape of the growth curve) were largely similar between control and chilled trees with no abrupt 298 reduction during the chilling (Fig. 2A). However, we did observe a 12±4-day delay in the onset of wood 299 formation in chilled trees relative to control trees (see dots in Fig. 2A). 300 301 The estimated effect of the carbon supply gradient on mass growth was less clear than the effect on ring 302 width, but some changes in the underlying wood anatomy emerged (Table 1). Like ring width, mass

growth, based on a single end-of-season microcore, was substantially less at 0.5 m in chilled trees than

controls. In contrast to ring width, mass growth showed no significant increases between chilled and control trees at 1.5, 2.5 or 4.0 m (Fig. 2A). Wood anatomy showed substantial variation among trees and sampling dates (Table 1; SI 4). Strangely, both the vessel density (i.e., number of vessels per mm² cross-sectional) and the percentage of cell-wall area had a tendency to decline with carbon supply, whereas vessel lumen area was relatively constant across samples (Table 1). Vessels have a lower cell-wall to lumen area ratio than fibers. Thus, fewer vessels of similar size per cross-sectional area at higher carbon supply in chilled trees might be expected to result a higher overall percentage of cell-wall area. However, the estimated percentage of cell-wall area at higher carbon supply covaried positively with vessel density (Table 1). Although small, the net changes in the percentage of cell-wall area and large variability in wood anatomy attenuated treatment-induced differences in ring width at high carbon supply (Fig. 2A).

314 Changes to stem CO₂ efflux

Stem CO₂ efflux responded rapidly to the chilling treatment (Fig. 5). Within a week after the start of chilling, stem CO₂ efflux per unit stem surface area started diverging between chilled and control trees at all stem heights (Fig. 5). Reductions in CO₂ efflux in chilled compared to control trees averaged 52% below two restrictions (-0.43±0.22 µmol m⁻² s⁻¹), 26% below one restriction (-0.22±0.22 µmol m⁻² s⁻¹), and 38% above both restrictions (-0.31±0.22 µmol m⁻² s⁻¹) over the chilling period. Once the chilling was switched off, stem CO₂ efflux of chilled trees converged with the control group within one or two weeks below both one and two restrictions (Fig. 5). However, above the upper restriction stem CO₂ efflux of the chilled group increased strongly averaging about twice those of the control group for the next three months, before converging towards the end of the growing season (Fig. 5).

Leaf-level changes

In addition to multiple effects at the stem-level, we found an accumulation of leaf NSC, a down-regulation of photosynthetic capacity, and earlier leaf colouration and fall in chilled trees (Fig. 3 & 6). During the chilling, leaf NSC concentrations started to diverge between treatments, culminating in increases in leaf sugar and starch concentrations of +14% (0.65±0.25% dry weight) and +168% (1.31±0.31% dry weight) relative to the controls (Fig. 3). While we only we measured photosynthesis shortly after the summer solstice (i.e., last week of chilling, 29 Jun to 10 Jul; Fig. 1C) when leaf starch concentrations just started to diverge between treatments (Fig. 3), maximal rates of photosynthetic electron transport (J_{max}) and RuBisCO carboxylase activity (V_{cmax}) as estimated from A/Ci curves declined with chilling (Fig. 6): V_{cmax} was 46.6±1.5 μmol m⁻² s⁻¹ for chilled trees compared with 52.1±1.7 μmol m⁻² s⁻¹ for control trees, J_{max} was 85 μmol m⁻² s⁻¹ for chilled compared to 97 μmol m⁻² s⁻¹ for control trees, and dark respiration was 5% higher in chilled trees relative to control (Fig. 6). Despite these

differences in photosynthetic parameters, we did not detect any changes in instantaneous photosynthetic rates or light response curves between the two treatments (SI 2). Likewise, we did not detect a significant treatment effect on ratios of variable fluorescence over maximum fluorescence in dark-adapted leaves (SI 2). In addition to changes in leaf NSCs and photosynthetic capacity, we also observed significantly earlier leaf coloration by 12±2 days and leaf fall by 16±2 days for chilled trees compared to control trees (Fig. 3). There were no effects of chilling on the tree water status as per leaf and branch water potentials and sap flow measurements (SI 3).

343

344

345

346

347

348

349

350

351

352

353

354

355

356

357

358

359

360

361

362

363

364

365

366

342

336

337

338

339

340

341

Discussion

Phloem carbon supply determines early-season wood growth

The pronounced local differences in final ring width along the carbon supply gradient suggest a direct supply-limitation in the early-growing season (C₁ in Fig. 1A). The effect is unlikely to be a direct coldinhibition of growth, as the cooling very localised (e.g., only 2.3°C difference to ambient at 1.5 m) and a direct cold inhibition would have affected all sampling height equally, being equidistant to the cooling collars. Natural and artificial defoliation experiments support the idea that reduced carbon supply can limit wood formation (Deslauriers et al., 2015; Wiley et al., 2017; Castagneri et al., 2020). Previous phloem transport experiments have also shown that ring width is affected by both low and high carbon supply (Wilson, 1968; Goren et al., 2004; Maier et al., 2010). We have previously shown that both ring width and biomass of white pine respond to mid- to late-season girdling and phloem compression (Rademacher et al., 2021a). The fact that we saw a much clearer effect on ring width may be due to the early season timing of the treatment, when effects on cell division and elongation are likely more pronounced than on cell-wall thickening, hence mass increment. Effects on volume growth have also been shown to be particularly strong in the early season under drought stress (D'Orangeville et al., 2018) and phloem transport manipulations (Maier et al., 2010; De Schepper et al., 2011). A treatment effect on carbon sequestration (i.e., mass growth) instead of ring width (i.e., volume growth) was only detectable in the present study under severe carbon supply-limitation below two chilling collars, with no clear effect at increased carbon supply. This could suggest that trees operate close to C*, which seems a likely evolutionary outcome given a co-limited process (e.g., McMurtrie & Dewar, 2013; Franklin et al., 2020); however, maintenance of such as joint limitation would require regulating feedbacks. Overall, we conclude that volume growth (and possibly mass growth) in red maple exhibit carbon supply-limitations in the early growing season.

Although ring width was associated with the spatial carbon supply gradient, there was no abrupt halt or reduction in growth as a result of the chilling. In fact, the shape of the intra-annual growth curve was similar for both treatments (Fig. 2A). Intra-annual wood development in conifers is known to be strongly constrained by endogenous factors, which results in typical gradual transitions of cell characteristics in seasonally-limited habitats (Buttò et al., 2020, 2021). The smooth shape of the observed intra-annual growth curve, despite the abrupt chilling and hence phloem transport restriction, supports an important role of endogenous factors on wood formation in this diffuse-porous angiosperm. Investigating xylogenesis and resulting anatomy in angiosperms is still rare (Balzano et al., 2018; Arnič et al., 2021) and comparing angiosperms and conifers is not simple, because off important physiological differences, such as a higher proportion of parenchyma cells in angiosperms (Spicer, 2014). While anatomical characteristics where not the primary focus of this work, we found little evidence for carbon supplyrelated changes in vessels density and the characteristics of fibers. Mean supply of carbon to the cambium has been shown to mainly affect cell division rate for white pine (Rademacher et al., 2021a), and the most parsimonious explanation for our results are systematic changes in cell proliferation rate (i.e., both fibers and vessels), thus cell numbers, with carbon supply rate. We did not detect an effect of carbon supply on the ratio of vessel to fibers, but these results are inconclusive due to the large between-sample variability. Differences in the sensitivities of vessel and fiber formation to carbon supply in angiosperms may have important consequences for water transport and carbon sequestration, thus presenting an important avenue of further research. Because systematic changes in wood anatomy with carbon supply would change the relationships between ring width (e.g., the most prevalent measure of wood growth) and mass, they could prove important in understanding how much carbon will be sequestered by non-coniferous trees in the future.

390391

392

393

394

395

396

397

398

399

400

401

368

369

370

371

372

373

374

375

376

377

378

379

380

381

382

383

384

385

386

387

388

389

Carbon supply and temperature have both also been found to influence the critical dates and dynamics of wood formation (Funada *et al.*, 2001; Rossi *et al.*, 2008; Rohde *et al.*, 2011; Cuny & Rathgeber, 2016; Balducci *et al.*, 2016). While the effect of temperature on the onset of wood formation is generally assumed to be cumulative over the dormancy period (Huang *et al.*, 2020), we observed a delay in the onset of wood growth in chilled trees although bud break had occurred roughly at the same time as the controls, possibly suggesting immediate and direct effect of temperature on cambial activation.

Alternatively, local changes in phloem NSC concentrations could be responsible for the different timings, as NSC reserves have been linked to resumption of growth for several angiosperms (Amico Roxas *et al.*, 2021). Reserves were also important in *Larix*, where in a cambial heating experiment, cambial activity resumed but then stopped when local starch reserves were used up (Oribe & Funada, 2017). However, carbon supply only changed gradually once the transport bottleneck was induced and phloem sugar

concentrations had not diverged yet between chilled and control trees. Moreover, the delay was similar across sampling heights, but the carbon supply and temperature gradients were not. Consequently, some additional signal is required to explain consistent delay along the stem or this may simply be a pre-existing between-group difference. Targeted manipulative experiments to better understand the role of temperature and carbon status on wood phenology at various points throughout the growing season, especially in angiosperms, are clearly still needed.

Sink feedbacks down-regulate source activity

Our findings at the stem-level provide strong evidence for a direct control of carbon supply on lateral meristem activity for red maple in the early growing season, yet we also found multiple lines of evidence for source-sink feedbacks. Looking at source tissues in leaves, we found an accumulation of NSCs, a down-regulation of photosynthetic capacity, and a shortened leaf season for the chilled trees, all suggesting a coupling between the supply-controlled lateral meristem and source tissues. We saw cumulative increases in leaf sugar and starch concentrations of the chilled trees compared to the control group, culminating in large differences towards the end of the season (Fig. 3). Although trees appear to be able to load the phloem against strong concentrations gradients (Gersony et al., 2021), the gradual NSC accumulation in leaves over the season presumably resulted from the backup of carbon transport in the phloem in chilled red maple, which is best characterised as a passive phloem loader (Eschrich & Fromm, 1994) like about half of all characterised tree species (Liesche, 2017). Higher NSC concentrations in turn have been theorized to inhibit photosynthesis (Salmon et al., 2020), which has long been confirmed in herbaceous plants and tree leaves (Vaughn et al., 2002; Iglesias et al., 2002), but lacked evidence along the long transport pathways between the cambium and canopy of mature trees. We only measured photosynthesis during the last week of chilling, when leaf sugar and starch concentrations just started to diverge between the chilled and control trees. Arguably, leaf NSC concentrations had not increased sufficiently to result in a detectable change in instantaneous photosynthetic rates or light response curves. Nonetheless, we already observed declines in the photosynthetic capacity (i.e., J_{max} and V_{cmax}).

Beyond the changes in photosynthetic capacity, increased leaf NSC concentrations may have caused the significant observed advancement of leaf coloration and fall for chilled trees compared to controls. This advancement stands in contrast to very similar dates of leaf colouration and fall in the previous year. This effect on leaf phenology is very unlikely to have arisen from a direct temperature-limitation, because chilling ended almost three months before leaf colouration and was limited to small parts of the stem. Accumulation of NSCs towards the end of the season has previously been linked to advancement of leaf

colouration and fall in the closely related sugar maple (Murakami et al., 2008), yet free-air CO₂ enrichment experiments consistently observe increases in photosynthesis, hence carbon supply, without clear advancement of leaf colouration or fall (Norby, 2021). The apparent discrepancy may be reconciled if the accumulation of leaf NSC causes the observed effects on leaf phenology directly, as such an accumulation has generally not been observed in free-air CO₂ enrichment experiments (Norby, 2021). Here, radial growth above both restrictions may have attained an upper limit (e.g., G_{max} in Fig. 1A), which led to the tree shifting from being source-limited (C₁) to sink-limited (C₂). This would suggest that the trees were operating close to C* (Fig. 1A). NSC may have accumulated in the phloem and leaves, as a consequence of this growth limitation. Independent of what caused the increase in leaf NSCs, the observed advancement of leaf phenology constitutes a third indication of source-sink coupling, whereby leaf-on period, hence source activity, is constrained due to a carbon-mediated feedback from sinks. Although the differences in photosynthetic capacity between the two groups did not lead to marked differences in instantaneous assimilation rates in the last week of chilling, they may have increased later in the growing season (concurrently with the observed gradual leaf NSC accumulation) and could sum to a substantial difference in carbon fixation over the entire growing season. Any effect on carbon assimilation would be compounded by the advanced leaf coloration and fall. Together the increases in leaf NSCs, the early down-regulation of photosynthetic capacity, and the advancement of autumn leaf phenology provide strong evidence for a feedback inhibition in mature forest trees.

Leaf NSC concentrations changed gradually over the entire growing season, whereas stem CO₂ efflux responded much quicker to the chilling treatment. These varying response scales highlight the need for continuous monitoring to be able to disentangle the complexity of the observed experimental effects. Carbon supply can either be sourced directly from recent assimilates or from NSC reserves, that can build up and be remobilized over multiple years (Carbone *et al.*, 2013; Muhr *et al.*, 2016). Like in other phloem transport manipulations (Maier *et al.*, 2010; Regier *et al.*, 2010; Rademacher *et al.*, 2021a), bulk NSC concentrations in stems and roots (here measured in the first centimetre of the stem and roots) reacted more sluggishly and show little to no treatment effect (Fig. 4). However, below both restrictions NSC remobilization and/or reduced sink activity compensated for the reduced phloem carbon transport to maintain phloem sugar concentrations. This supports the idea that at low carbon supply, sugar concentrations near the cambium are homeostatically maintained within relatively tight limits that vary seasonally (Rademacher *et al.*, 2021a; Huang *et al.*, 2021). Such homeostasis is typical in biological systems and likely evolved to ensure metabolic stability for inter-annual wood formation given the role of

Local carbon dynamics show temporal decoupling of treatment effects

soluble sugar concentrations as a signal, resource and possible driver of wood formation (Riou-Khamlichi et al., 2000; Lastdrager et al., 2014; Cartenì et al., 2018). Across the developing xylem, NSC concentrations vary markedly (Uggla et al., 2001). Given that we observed contrasting reactions of NSCs in adjacent tissues, such as phloem and stem soluble sugar, it begs the question whether these gradients remain stable under varying conditions or whether only particular aspects of the gradient, such as phloem concentrations, are maintained. Repeated and spatially highly resolved measurements of NSC concentrations, using techniques such as Raman spectroscopy (Gersony et al., 2021), promise to advance our understanding of these gradients and their dynamics in response to internal and external factors. These gradients are likely to be crucial to understanding the impact of carbon dynamics specific processes of wood formation (e.g., cambial activity, cell enlargement, and cell-wall thickening). In contrast to reduced carbon supply, we did not observe a substantial accumulation of bulk NSCs in stems at elevated carbon supply throughout the growing season. While this can be interpreted as further evidence that the cambium is carbon supply-limited (e.g., any additional carbon is used for growth; C₁), some coordination is needed to avoid the depletion of reserves that are crucial for winter survival (Vitasse et al., 2014), spring emergence (Amico Roxas et al., 2021), and defense against various stressors (Wiley et al., 2017). Nonetheless, our findings support the idea that NSC reserves are not simply an overflow store of energy (Martínez-Vilalta et al., 2016) that can be tapped into quasi-instantaneously, as they remain very stable even when carbon import is acutely restricted.

The observed changes in stem CO₂ efflux correspond to imposed temperatures during the chilling period and then the carbon supply gradient thereafter, suggesting that local metabolic activity is more sensitive to changes in temperature than to changes in carbon supply. Nonetheless, the spike in CO₂ efflux post-chilling supports that the idea that the first pulse of phloem-transported carbon after the restriction is lifted is metabolized locally (possibly to fuel wall-thickening). Measurements of CO₂ efflux may include some portion that is transported in the xylem from adjacent regions (Teskey et al., 2008). However, given that xylem transported CO₂ has been shown to decrease in trees with severed phloem transport (Bloemen *et al.*, 2014), and CO₂ solubility decreases with temperature (Servio & Englezos, 2001), we suspect that the observed changes in CO₂ efflux mainly represent local metabolic activity. Respiration is long known to respond to both temperature and substrate concentrations (Amthor, 2000). The observed pattern is likely a combination of reduced respiration during the chilling and a spike in metabolic activity as a response to stopping the chilling. Interestingly, the large and immediate changes in CO₂ efflux suggest that local metabolic activity and growth can be somewhat decoupled temporarily or spatially, as CO₂ efflux was lower when radial volume growth was higher at high carbon supply (e.g., 2.5 m) in chilled trees relative to control during the chilling period. Given that trees seem to operate close to C* (Fig. 1A),

understanding the regulating interactions between sources and sinks is a key component of understanding the mechanisms of wood formation.

504

505

506

507

508

509

510

511

512

513

514

515

516

517

518

519

520

521

522

523

524

525

502

503

Conclusions

We found evidence for a carbon supply-limitation of the activity of the lateral meristem as well as multiple source-sink feedbacks in mature red maple trees. These feedbacks can reconcile the apparent discrepancy arising from previous phloem transport manipulations (Wilson, 1968; De Schepper et al., 2011; Rademacher et al., 2021a) and defoliation experiments (Deslauriers et al., 2015; Castagneri et al., 2020) that showed carbon supply-limitation of the lateral meristem, and whole-tree level CO₂ enrichment that suggested a sink-limitation at increased carbon supply (Körner et al., 2005). Our results illustrate how within-tree feedbacks can reduce carbon assimilation when phloem sugar concentrations increase as a result of phloem transport manipulations in mature red maples. These findings suggest that trees operate close to both source- and sink-limitation and may switch between them. While our results are based on a single species at one location, they identify potential mechanisms for reconciling apparently contrasting evidence with regard to the control of wood growth. More work is needed to evaluate whether these findings can be extrapolated to other species, sites, ecosystem, environmental conditions, or even periods of the season. Our work highlights the need to integrate evidence from multiple tissues (i.e., leaves and phloem, xylem in stems and roots) across entire growing seasons when investigating source-sink interactions. Otherwise, conclusions about source-sink interactions (e.g., from single tissues or over short periods) can be mistaken because local and whole-tree effects can be temporarily decoupled, as found here. Importantly, our identification of strong source-sink interactions even in unstressed conditions refute the prevailing source-centric paradigm as used in most current models representing mature trees in natural settings.

Acknowledgement

Tim Rademacher, Andrew D. Richardson, Andrew D. Friend, and Yizhao Chen acknowledge support from the Natural Environment Research Council—National Science Foundation International Collaboration programme under grants nos. NE/P011462/1 and DEB-1741585. Andrew D. Richardson and Tim Rademacher also acknowledge the support from the National Science Foundation under grants DEB-1237491 and DEB-1832210. We thank David Basler, Teemu Hölltä, Henrik Hartmann and Christian Körner for discussion of the ideas, Mark von Scoy, Elise Miller, and Shawna Greyeyes for help

- 532 in the field, and Shawna Greyeyes, Amberlee Pavey and Angelina Valenzuela for help in the laboratory.
- We also thank David Basler for sharing the orthomosaics of the site.

- 535 Author Contributions
- Tim Rademacher and Andrew D. Richardson designed the experiment with input from James M.
- LeMoine, Andrew D. Friend, Yizhao Chen, Patrick Fonti, and Annemarie H. Eckes-Shephard. Tim
- Rademacher and Franics Bowles built the chilling apparatus. Tim Rademacher conducted and supervised
- the field work. Tim Rademacher, Marina V. Fonti, James M. LeMoine and Patrick Fonti processed the
- samples. Tim Rademacher analysed the data, produced the figures and wrote a first draft. All co-authors
- discussed ideas, provided feedback, edited the manuscript draft and approved the manuscript for
- submission.

543

544 References

- 1. Pan, Y. et al. A Large and Persistent Carbon Sink in the World's Forests. Science 333, 988–
- 547 993 (2011).
- 548 2. Ballantyne, A. P., Alden, C. B., Miller, J. B., Tans, P. P. & White, J. W. C. Increase in
- observed net carbon dioxide uptake by land and oceans during the past 50 years. *Nature* **488**,
- 550 70–72 (2012).
- 3. Brienen, R. J. W. et al. Forest carbon sink neutralized by pervasive growth-lifespan trade-
- offs. Nat. Commun. 11, 4241 (2020).
- 553 4. Fritts, H. C. *Tree Rings and Climate*. (Elsevier, 1976). doi:10.1016/B978-0-12-268450-
- 554 0.X5001-0.
- 555 5. Friedlingstein, P. et al. Global Carbon Budget 2020. Earth Syst. Sci. Data 12, 3269–3340
- 556 (2020).
- 6. Fatichi, S., Leuzinger, S. & Körner, C. Moving beyond photosynthesis: from carbon source

- to sink-driven vegetation modeling. New Phytol. 201, 1086–1095 (2014).
- 7. Zuidema, P. A., Poulter, B. & Frank, D. C. A Wood Biology Agenda to Support Global
- Vegetation Modelling. *Trends Plant Sci.* **23**, 1006–1015 (2018).
- 8. Friend, A. D. et al. On the need to consider wood formation processes in global vegetation
- models and a suggested approach. Ann. For. Sci. 76, 49 (2019).
- 9. Gessler, A. & Grossiord, C. Coordinating supply and demand: plant carbon allocation
- strategy ensuring survival in the long run. New Phytol. 222, 5–7 (2019).
- 10. Körner, C. Plant CO₂ responses: an issue of definition, time and resource supply. *New*
- 566 *Phytol.* **172**, 393–411 (2006).
- 11. Pugh, T. A. M. et al. Role of forest regrowth in global carbon sink dynamics. *Proc. Natl.*
- 568 Acad. Sci. 116, 4382–4387 (2019).
- 12. Hartmann, H. et al. Identifying differences in carbohydrate dynamics of seedlings and
- mature trees to improve carbon allocation in models for trees and forests. *Environ. Exp. Bot.*
- **152**, 7–18 (2018).
- 13. Luo, Y. et al. Elevated Co2 Differentiates Ecosystem Carbon Processes: Deconvolution
- Analysis of Duke Forest Face Data. Ecol. Monogr. 71, 357–376 (2001).
- 574 14. Castagneri, D. et al. Long-Term Impacts of Defoliator Outbreaks on Larch Xylem Structure
- and Tree-Ring Biomass. Front. Plant Sci. 11, (2020).
- 576 15. Deslauriers, A., Caron, L. & Rossi, S. Carbon allocation during defoliation: testing a
- defense-growth trade-off in balsam fir. Front. Plant Sci. 6, (2015).
- 578 16. Wilson, B. F. Effect of girdling on cambial activity in white pine. Can. J. Bot. 46, 141–146
- 579 (1968).
- 580 17. Ainsworth, E. A. & Long, S. P. What have we learned from 15 years of free-air CO₂

- enrichment (FACE)? A meta-analytic review of the responses of photosynthesis, canopy
- properties and plant production to rising CO₂. New Phytol. **165**, 351–372 (2005).
- 18. Körner, C. et al. Carbon Flux and Growth in Mature Deciduous Forest Trees Exposed to
- 584 Elevated CO₂. *Science* **309**, 1360–1362 (2005).
- 585 19. Salmon, Y. et al. Leaf carbon and water status control stomatal and nonstomatal limitations
- of photosynthesis in trees. *New Phytol.* **226**, 690–703 (2020).
- 587 20. Rademacher, T. et al. Using Direct Phloem Transport Manipulation to Advance
- Understanding of Carbon Dynamics in Forest Trees. Front. For. Glob. Change 2, (2019).
- 589 21. Rossi, S., Anfodillo, T. & Menardi, R. Trephor: A New Tool for Sampling Microcores from
- tree stems. *IAWA J.* 89–97 (2006) doi:10.1163/22941932-90000139.
- 591 22. von Arx, G. & Carrer, M. ROXAS A new tool to build centuries-long tracheid-lumen
- 592 chronologies in conifers. *Dendrochronologia* **32**, 290–293 (2014).
- 593 23. Jensen, K. H. et al. Sap flow and sugar transport in plants. Rev. Mod. Phys. 88, (2016).
- 594 24. Gould, N., Minchin, P. E. H. & Thorpe, M. R. Direct measurements of sieve element
- 595 hydrostatic pressure reveal strong regulation after pathway blockage. Funct. Plant Biol. 31,
- 596 987 (2004).
- 597 25. Thorpe, M. R. et al. Rapid cooling triggers for isome dispersion just before phloem transport
- 598 stops. *Plant Cell Environ.* **33**, 259–271 (2010).
- 599 26. Peuke, A. D., Windt, C. & Van As, H. Effects of cold-girdling on flows in the transport
- phloem in Ricinus communis: is mass flow inhibited? *Plant Cell Environ.* **29**, 15–25 (2006).
- 27. Amthor, J. S. The McCree–de Wit–Penning de Vries–Thornley respiration paradigms: 30
- 602 years later. *Ann. Bot.* **86**, 1–20 (2000).
- 28. Rademacher, T. et al. Manipulating phloem transport affects wood formation but not local

- nonstructural carbon reserves in an evergreen conifer. *Plant Cell Environ.* **44**, 2506–2521
- 605 (2021).
- 606 29. Buttò, V., Rozenberg, P., Deslauriers, A., Rossi, S. & Morin, H. Environmental and
- developmental factors driving xylem anatomy and micro-density in black spruce. New
- 608 *Phytol.* **230**, 957–971 (2021).
- 30. Buttò, V. et al. The role of plant hormones in tree-ring formation. Trees 34, 315–335 (2020).
- 31. Funada, R., Kubo, T., Tabuchi, M., Sugiyama, T. & Fushitani, M. Seasonal Variations in
- Endogenous Indole-3-Acetic Acid and Abscisic Acid in the Cambial Region of Pinus
- densiflora Sieb. et Zucc. Stems in Relation to Earlywood-Latewood Transition and Cessation
- of Tracheid Production. *Holzforschung* **55**, (2001).
- 32. Rossi, S. *et al.* Critical temperatures for xylogenesis in conifers of cold climates. *Glob. Ecol.*
- 615 *Biogeogr.* **17**, 696–707 (2008).
- 33. Rohde, A., Bastien, C. & Boerjan, W. Temperature signals contribute to the timing of
- photoperiodic growth cessation and bud set in poplar. *Tree Physiol.* **31**, 472–482 (2011).
- 618 34. Frankenstein, C., Eckstein, D. & Schmitt, U. The onset of cambium activity A matter of
- agreement? Dendrochronologia 23, 57–62 (2005).
- 620 35. Huang, J.-G. et al. Photoperiod and temperature as dominant environmental drivers
- triggering secondary growth resumption in Northern Hemisphere conifers. *Proc. Natl. Acad.*
- 622 *Sci.* **117**, 20645–20652 (2020).
- 623 36. Amico Roxas, A., Orozco, J., Guzmán-Delgado, P. & Zwieniecki, M. A. Spring phenology is
- affected by fall non-structural carbohydrate concentration and winter sugar redistribution in
- three Mediterranean nut tree species. *Tree Physiol.* tpab014 (2021)
- doi:10.1093/treephys/tpab014.

- 37. Huang, J. et al. Storage of carbon reserves in spruce trees is prioritized over growth in the
- face of carbon limitation. *Proc. Natl. Acad. Sci.* **118**, (2021).
- 38. Riou-Khamlichi, C., Menges, M., Healy, J. M. S. & Murray, J. A. H. Sugar Control of the
- Plant Cell Cycle: Differential Regulation of Arabidopsis D-Type Cyclin Gene Expression.
- 631 *Mol. Cell. Biol.* **20**, 4513–4521 (2000).
- 632 39. Lastdrager, J., Hanson, J. & Smeekens, S. Sugar signals and the control of plant growth and
- 633 development. J. Exp. Bot. 65, 799–807 (2014).
- 40. Cartenì, F. et al. The Physiological Mechanisms Behind the Earlywood-To-Latewood
- Transition: A Process-Based Modeling Approach. Front. Plant Sci. 9, (2018).
- 41. Dietze, M. C. et al. Nonstructural Carbon in Woody Plants. Annu. Rev. Plant Biol. 65, 667–
- 637 687 (2014).
- 638 42. Uggla, C., Magel, E., Moritz, T. & Sundberg, B. Function and Dynamics of Auxin and
- 639 Carbohydrates during Earlywood/Latewood Transition in Scots Pine. *Plant Physiol.* **125**,
- 640 2029–2039 (2001).
- 43. Gersony, J. T., McClelland, A. & Holbrook, N. M. Raman spectroscopy reveals high phloem
- sugar content in leaves of canopy red oak trees. *New Phytol.* **232**, 418–424 (2021).
- 643 44. Walker, A. P. et al. Integrating the evidence for a terrestrial carbon sink caused by increasing
- atmospheric CO₂. New Phytol. **229**, 2413–2445 (2021).
- 45. Baker, N. R. & Rosenqvist, E. Applications of chlorophyll fluorescence can improve crop
- production strategies: an examination of future possibilities. J. Exp. Bot. 55, 1607–1621
- 647 (2004).
- 46. Groom, Q. J. & Baker, N. R. Analysis of Light-Induced Depressions of Photosynthesis in
- Leaves of a Wheat Crop during the Winter. *Plant Physiol.* **100**, 1217–1223 (1992).

- 47. Kitajima, M. & Butler, W. L. Quenching of chlorophyll fluorescence and primary
- photochemistry in chloroplasts by dibromothymoquinone. Biochim. Biophys. Acta BBA -
- 652 Bioenerg. **376**, 105–115 (1975).
- 48. Schaberg, P. G., Murakami, P. F., Butnor, J. R. & Hawley, G. J. Experimental branch
- 654 cooling increases foliar sugar and anthocyanin concentrations in sugar maple at the end of
- 655 the growing season. Can. J. For. Res. 47, 696–701 (2017).
- 49. Norby, R. J. Comment on "Increased growing-season productivity drives earlier autumn leaf
- senescence in temperate trees". *Science* **371**, eabg1438 (2021).
- 50. Norby, R. J., Warren, J. M., Iversen, C. M., Medlyn, B. E. & McMurtrie, R. E. CO2
- enhancement of forest productivity constrained by limited nitrogen availability. *Proc. Natl.*
- 660 Acad. Sci. 107, 19368–19373 (2010).
- 51. De Schepper, V., Vanhaecke, L. & Steppe, K. Localized stem chilling alters carbon
- processes in the adjacent stem and in source leaves. *Tree Physiol.* **31**, 1194–1203 (2011).
- 52. De Schepper, V., De Swaef, T., Bauweraerts, I. & Steppe, K. Phloem transport: a review of
- mechanisms and controls. *J. Exp. Bot.* **64**, 4839–4850 (2013).
- 53. Davidson, A., Keller, F. & Turgeon, R. Phloem loading, plant growth form, and climate.
- 666 Protoplasma **248**, 153–163 (2011).
- 54. Maier, C. A., Johnsen, K. H., Clinton, B. D. & Ludovici, K. H. Relationships between stem
- 668 CO2 efflux, substrate supply, and growth in young loblolly pine trees. *New Phytol.* **185**,
- 669 502–513 (2010).
- 55. Boose, E. & Gould, E. Harvard Forest Climate Data since 1964.
- https://harvardforest.fas.harvard.edu/exist/apps/datasets/showData.html?id=hf300 (2019).
- 56. Rademacher, T. et al. The Wood Image Analysis and Dataset (WIAD): Open-access visual

- analysis tools to advance the ecological data revolution. *Methods Ecol. Evol.* **n/a**, (2021).
- 57. Seyednasrollah, B., Rademacher, T. T. & Basler, D. bnasr/wiad: Wood Image Analysis and
- 675 Dataset (WIAD) Source Code. (Zenodo, 2021). doi:10.5281/zenodo.5272692.
- 58. Cuny, H. E. et al. Generalized additive models reveal the intrinsic complexity of wood
- 677 formation dynamics. J. Exp. Bot. **64**, 1983–1994 (2013).
- 678 59. Pya, N. scam: Shape Constrained Additive Models. (2020).
- 679 60. Lindeberg, T. Image Matching Using Generalized Scale-Space Interest Points. *J. Math.*
- 680 *Imaging Vis.* **52**, 3–36 (2015).
- 681 61. Barthelme, S. imager: Image Processing Library Based on 'CImg'. (2020).
- 682 62. Kellogg, R. M. & Wangaard, F. F. Variation in The Cell-Wall Density of Wood. Wood Fiber
- 683 *Sci.* **1**, 180–204 (1969).
- 684 63. Chow, P. S. & Landhausser, S. M. A method for routine measurements of total sugar and
- starch content in woody plant tissues. *Tree Physiol.* **24**, 1129–1136 (2004).
- 686 64. Carbone, M. S. et al. Flux Puppy An open-source software application and portable system
- design for low-cost manual measurements of CO2 and H2O fluxes. *Agric. For. Meteorol.*
- 688 **274**, 1–6 (2019).
- 689 65. Perez-Priego, O. et al. Sun-induced chlorophyll fluorescence and photochemical reflectance
- index improve remote-sensing gross primary production estimates under varying nutrient
- availability in a typical Mediterranean savanna ecosystem. *Biogeosciences* **12**, 6351–6367
- 692 (2015).
- 693 66. O'Keefe, J. Phenology of Woody Species at Harvard Forest since 1990.
- https://harvardforest1.fas.harvard.edu/exist/apps/datasets/showData.html?id=hf003 (2019).
- 695 67. Duursma, R. A. Plantecophys An R Package for Analysing and Modelling Leaf Gas

- 696 Exchange Data. *PLoS ONE* **10**, e0143346 (2015).
- 697 68. Maxwell, K. & Johnson, G. N. Chlorophyll fluorescence—a practical guide. J. Exp. Bot. 51,
- 698 659–668 (2000).

- 699 69. R Core Team. R: A Language and Environment for Statistical Computing. (R Foundation for
- 700 Statistical Computing, 2019).
- 70. Bates, D., Mächler, M., Bolker, B. & Walker, S. Fitting Linear Mixed-Effects Models Using
- 702 lme4. J. Stat. Softw. 67, 1–48 (2015).
- 703 71. Saefken, B., Ruegamer, D., Kneib, T. & Greven, S. Conditional Model Selection in Mixed-
- To Effects Models with cAIC4. ArXiv E-Prints (2018).

Table and figure captions

Table 1 – Estimated treatment effects using a mixed effects model fitted using the restricted maximum likelihood procedure in the lme4 package (Bates et al., 2015) in R (R core team, 2019). Each model contained tree identifier as a random effect plus the listed intercepts and fixed effects for which we provide the mean effect, its standard error, and the t-value in the following format: $\mu \pm \sigma_{\mu}$ (t-value). "X" stands for chilled treatment (light blue cell background) and "C" for control treatment. "y2019" and "y2018" stand for categorical variable of year and sampling height are listed as 0.5 m (below restrictions), 1.5 m (in-between restrictions), 2.5 m and 4.0 m (above restrictions). We tested effects on ring width, vessel density (ρ_{Vessel}), estimated vessel radius (r_{Vessel}), estimated percentage cell-wall area, and estimated mass contained in ring (m) on the microcore images collected on the 2019-09-25.

Effect	Ring width (µm)	ęν _{essel} (n mm ⁻²)	r _{Vessel} (μm)	Percentage cell-wall area (%)	m (g cm²)
Intercept	858±804 (1.066)	80±13 (6.149)	22.7±1.8 (12.397)	43.9±3.3 (13.496)	0.43±0.03 (13.916)
y2019	1049±734 (1.429)	-28±14 (-2.043)	-1.4±1.3 (-1.119)	-9.5±3.6 (-2.613)	-0.09±0.04 (-2.543)
y2019 : X : 4.0 m	419±1137 (0.369)	-16±18 (-0.886)	-0.5±2.6 (-0.211)	-2.9±4.6 (-0.619)	-0.03±0.04 (-0.639)
y2019 : C : 2.5 m	696±734 (0.949)	14±14 (1.067)	-0.6±1.3 (-0.501)	0.9±3.6 (0.238)	0.01±0.04 (0.231)
y2019 : X : 2.5 m	284±1137 (0.250)	-11± 18 (-0.610)	0.2±2.6 (0.070)	2.1±4.6 (0.452)	0.02±0.04 (0.466)
y2019 : C : 1.5 m	-183±734 (-0.249)	-10±13 (-0.706)	1.2±1.4 (0.834)	1.5±3.6 (0.400)	0.01±0.04 (0.389)
y2019 : X : 1.5 m	-494±1137 (0.434)	-2±18 (-0.111)	2.7±2.6 (1.051)	7.5±4.6 (1.636)	0.07±0.04 (1.687)
y2019 : C : 0.5 m	-371±734 (-0.505)	-16±15 (-1.093)	0.2±1.3 (0.136)	-4.1±4.0 (-1.040)	-0.05±0.04 (-1.335)
y2019 : X : 0.5 m	-1567±1137 (-1.378)	3±18 (0.185)	1.1±2.6 (0.427)	5.0±4.6 (1.083)	0.05±0.04 (1.117)
y2018 : X : 4.0 m	-42±1137 (-0.037)	1±18 (0.036)	0.2±2.6 (0.091)	1.2±4.6 (0.260)	0.01±0.04 (0.268)
y2018 : C: 2.5 m	-74±734 (-0.101)	-29±14 (-2.096)	-0.3±1.3 (-0.267)	-9.6±3.6 (-2.632)	-0.09±0.04 (-2.562)
y2018 : X : 2.5 m	-29±1137 (-0.026)	-16±18 (-0.873)	2.4±2.6 (0.940)	1.5±4.6 (0.319)	0.01±0.04 (0.329)
y2018 : C : 1.5 m	-95±734 (-0.130)	-20±14 (-1.478)	1.0±1.4 (0.742)	-3.1±3.6 (-0.842)	-0.03±0.04 (-0.819)
y2018 : X : 1.5 m	-26±1137 (0.023)	-15±18 (-0.833)	2.7±2.6 (1.026)	2.2±4.6 (0.488)	0.02±0.04 (0.503)
y2018 : C : 0.5 m	166±734 (0.226)	-25±15 (-1.682)	2.5±1.3 (1.956)	-2.2±4.0 (-0.533)	0.00±0.04 (0.128)
y2018 : X : 0.5 m	653±1137 (0.574)	-23±18 (-1.222)	1.4±2.6 (0.548)	-0.8±4.6 (-0.177)	-0.01±0.04 (-0.182)

Figure 1 - (A) Conceptual responses of radial wood growth and photosynthesis to changes in carbon supply under supply- (turquoise lines; C_1) versus sink-limitation (purple lines; C_2) with orange shading indicating the overall limitation, which may switch over time. C^* indicates point were growth and photosynthesis switch between being supply- versus sink-limited. G_{max} indicates a theoretical maximum growth rate. (B) Experimental setup including tissue sampling locations, (C) timeline of treatments including start and end dates of chilling (grey vertical dashed lines), wood growth and NSC sampling dates (orange vertical lines), and the period of photosynthesis measurements (purple rectangle); and (D) mean temperatures for the air (red line), the phloem of chilled trees (blue line), and the phloem of control trees (green line).

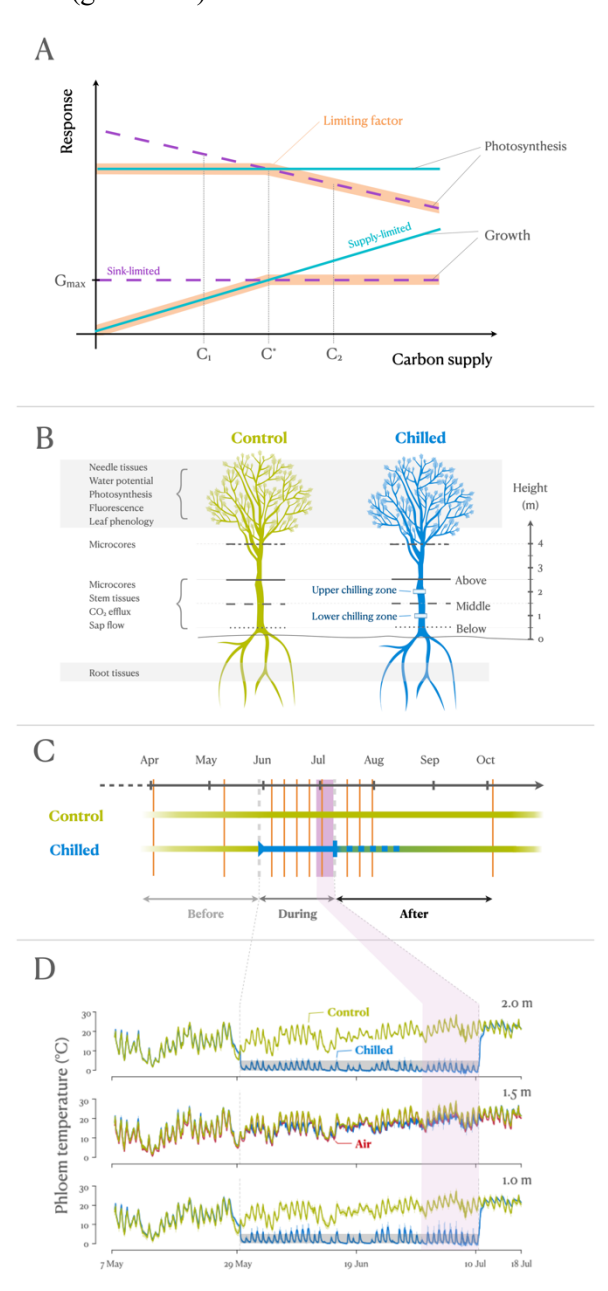
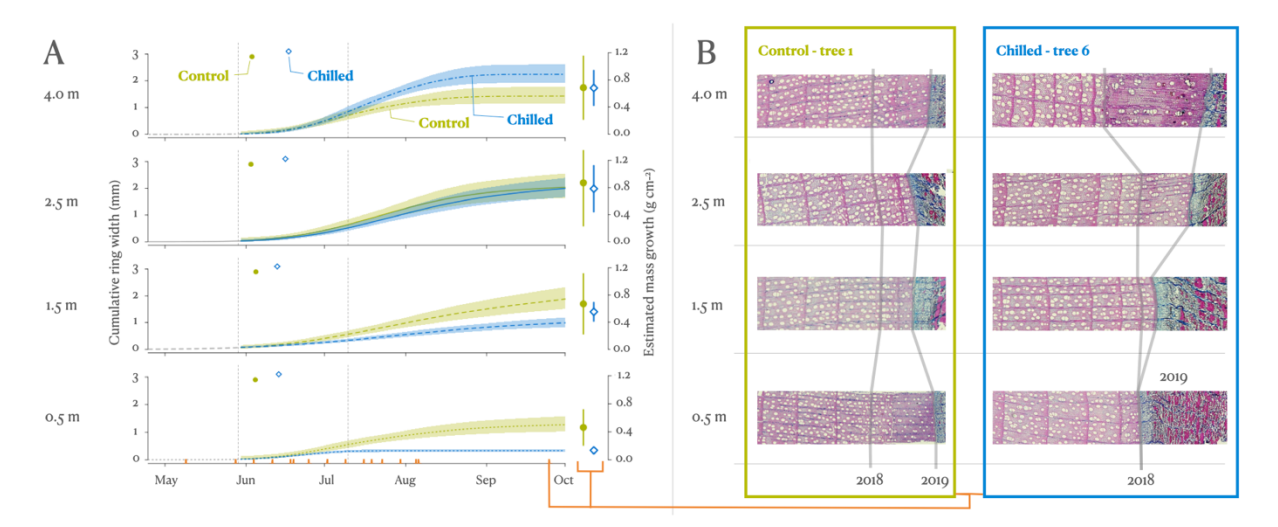
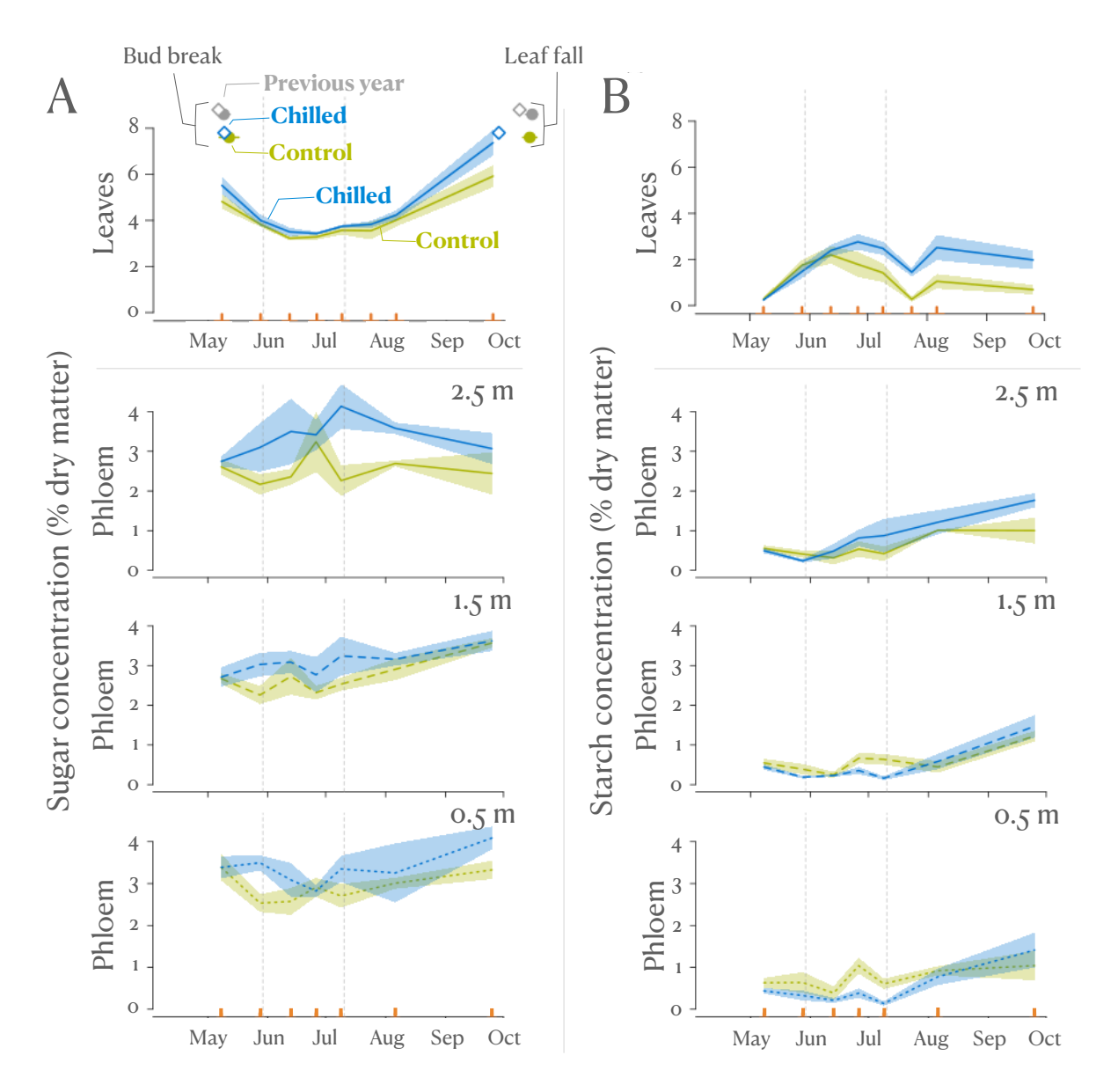


Figure 2 - (A) Dynamics of radial growth in chilled (blue) versus control trees (green) at 4.0, 2.5, 1.5, and 0.5 m. Lines and shading illustrate the mean and one standard error of a general additive model fitted to the four trees in each treatment. The mean start of the growing season (i.e., visual observation from microcores) is indicated at the top of each panel as small blue diamond for chilled trees and small green dots for control trees. The mean estimated annual radial mass increment per 1 cm² cross-sectional area (close to area of a typical increment core) and one standard error are displayed on the right as large blue diamonds and bars for chilled trees and large green dots and bars for control trees. Grey dashed vertical lines show the start and end of the chilling period and orange tick marks on the x-axis denote sampling dates. (B) Images of thin-sections from the 25th September for one control (tree 1 on left) and chilled tree (tree 6 on right). The images were rescaled to keep growth of the previous years relatively constant. The two grey lines indicate the final ring boundaries of the 2018 and 2019 rings, demarcating the growing season that included our chilling experiment. A high-resolution version of the images with more details can be found in the supplements (SI 4).





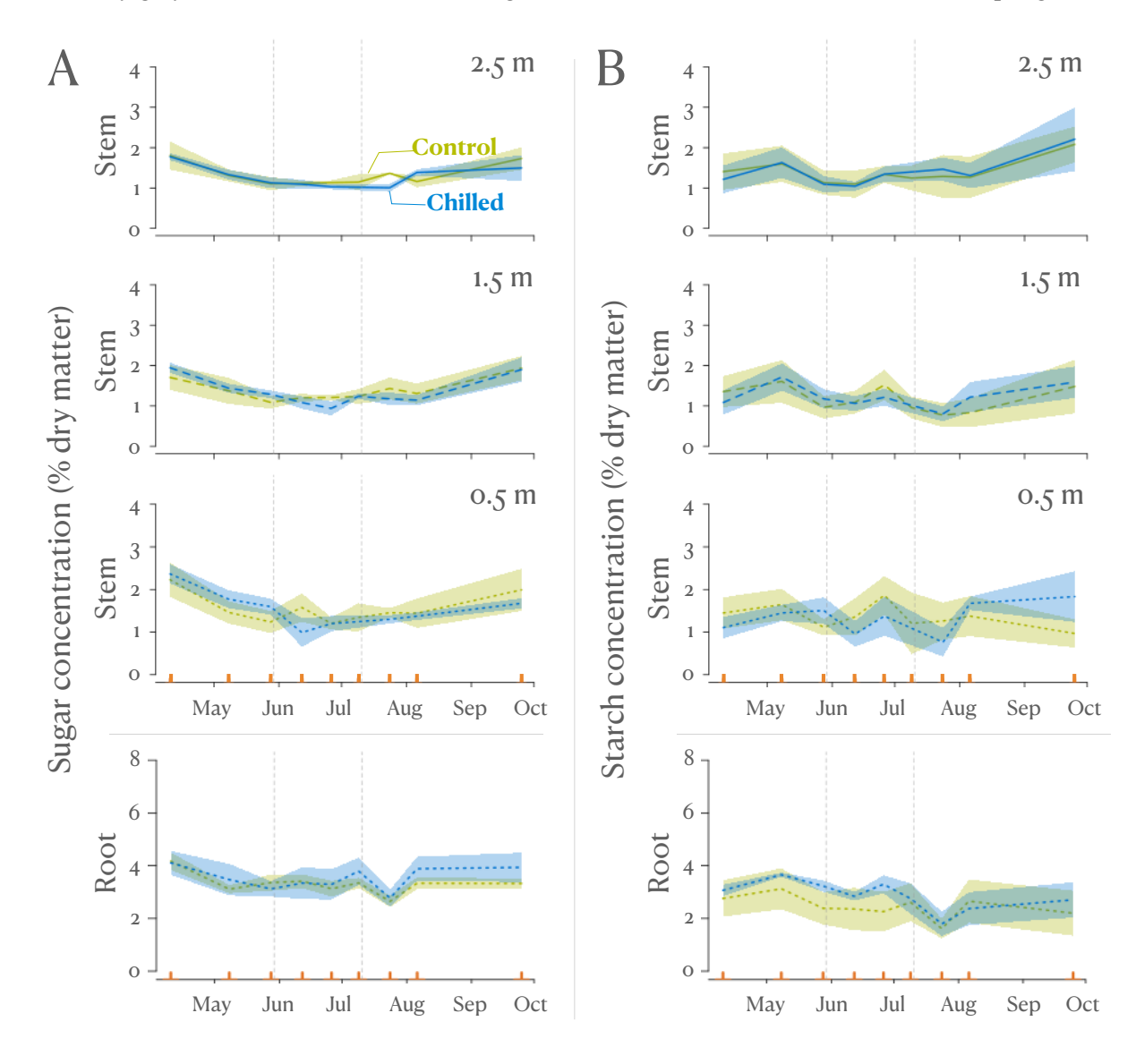


Figure 5 - Weekly mean stem CO₂ efflux rates on a stem-area basis for chilled (blue lines) and control trees (green lines) as measured throughout the season. Shading displays one standard error of the mean. The switching on and off of the chilling is indicated by grey vertical dashed lines and orange tick marks on the x-axis denote sampling dates.

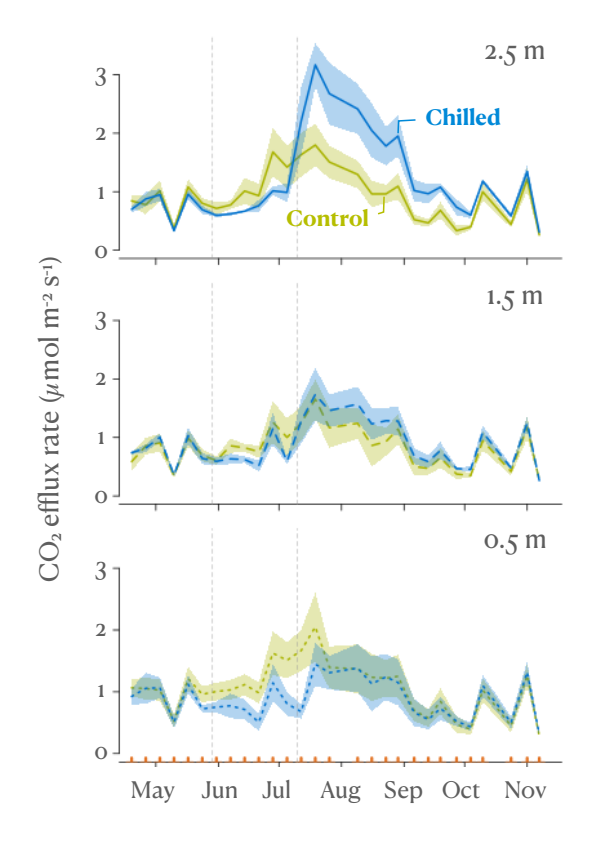


Figure 6 - (A) A/Ci curves of chilled (blue) and control trees (green) as measured during the last week of the chilling period. Line brightness corresponds to the limiting factor with dark lines showing V_{cmax} -limited curves, intermediate colours showing J_{max} -limited curves and bright lines showing the combined limitation. Control trees have slightly higher J_{max} and V_{cmax} values compared with chilled trees. (B) Paired measurements (n = 46) of instantaneous assimilation rates showed slightly higher rates for control trees (green dots) at the bottom of the canopy (open symbols) relative to chilled trees (blue diamonds), while sun-leaves (filled symbol) did not show any differences. Large symbols give the respective group mean for instantaneous rates (i.e., top chilled, bottom chilled, top control, and bottom control) in (B).

